Seasonal Prediction Skill of Northern Extratropical Surface Temperature Driven by the Stratosphere

LIWEI JIA,[a,b,f] XIAOSONG YANG,[c,b] GABRIEL VECCHI,[b] RICHARD GUDGEL,[b] THOMAS DELWORTH,[b] STEPHAN FUEGLISTALER,[d] PU LIN,[d] ADAM A. SCAIFE,[e] SETH UNDERWOOD,[b] AND SHIAN-JIANN LIN[b]

[a] *Princeton University, Princeton, New Jersey*
[b] *NOAA/Geophysical Fluid Dynamics Laboratory, Princeton, New Jersey*
[c] *University Corporation for Atmospheric Research, Princeton, New Jersey*
[d] *Atmospheric and Oceanic Sciences Program, Princeton University, Princeton, New Jersey*
[e] *Met Office Hadley Centre, Exeter, United Kingdom*

(Manuscript received 25 June 2016, in final form 7 March 2017)

ABSTRACT

This study explores the role of the stratosphere as a source of seasonal predictability of surface climate over Northern Hemisphere extratropics both in the observations and climate model predictions. A suite of numerical experiments, including climate simulations and retrospective forecasts, are set up to isolate the role of the stratosphere in seasonal predictive skill of extratropical near-surface land temperature. It is shown that most of the lead-0-month spring predictive skill of land temperature over extratropics, particularly over northern Eurasia, stems from stratospheric initialization. It is further revealed that this predictive skill of extratropical land temperature arises from skillful prediction of the Arctic Oscillation (AO). The dynamical connection between the stratosphere and troposphere is also demonstrated by the significant correlation between the stratospheric polar vortex and sea level pressure anomalies, as well as the migration of the stratospheric zonal wind anomalies to the lower troposphere.

1. Introduction

The predictability of seasonally averaged surface temperature and precipitation has long been known to arise from year-to-year variations of the ocean. Numerous studies have demonstrated the role of the tropical Pacific and its accompanying atmospheric component (known as ENSO) in seasonal prediction of temperature, precipitation, and many other essential climate variables (Lau 1985; Ropelewski and Halpert 1986; Stockdale et al. 1998; Shukla 1998; Wang et al. 2000; Jia et al. 2015; Yang et al. 2015). Compared to the close connection between tropical surface climate and ENSO, and skillful seasonal prediction of tropical climate in the current generation of global climate models, the connection between extratropical surface climate and ENSO is limited, and the predictive skill of surface climate over the extratropics, such as northern Eurasia, is much lower (Kryjov 2012). This suggests that, in order to extract seasonal prediction skill of surface climate over northern Eurasia, one must seek other drivers beyond tropical ocean–atmosphere coupling. The extratropical stratosphere, which has relatively long time scales of variability and has been shown to connect to the troposphere below it (Thompson et al. 2002; Cohen et al. 2007; Kidston et al. 2015; Baldwin et al. 2003), could serve as such a source of seasonal predictability over the extratropics. The stratospheric influence on the troposphere and surface climate can arise through fluctuations in the speed of the stratospheric circumpolar westerly jet (i.e., polar vortex) that forms in winter and spring. For example, over the Northern Hemisphere, a weakening of the stratospheric polar vortex shifts the tropospheric jet stream southward (often associated with the negative phase of the Arctic Oscillation), leading to low temperatures over northern Eurasia and the eastern United States (Thompson et al. 2002; Kidston et al. 2015).

Several studies have shown seasonal predictive skill of extratropical surface climate and atmospheric circulation such as the Arctic Oscillation (AO)/North Atlantic

[f] Current affiliation: Climate Prediction Center, NOAA/NWS/NCEP, College Park, and Innovim, LLC, Greenbelt, Maryland.

Corresponding author: Liwei Jia, liwei.jia@noaa.gov

DOI: 10.1175/JCLI-D-16-0475.1

TABLE 1. List of FLOR constrained experiments.

Expt name	Constraints	Radiative forcing	Time period	Ensemble size
SSTonly	SST relaxed to HadISST (5-day time scale)	Time varying	1981–2015	5
SST+Strat	SST relaxed to HadISST (5-day time scale); horizontal winds and temperatures above 100 hPa relaxed to MERRA (6-h time scale)	Time varying	1981–2015	5

Oscillation (NAO), but the source of the skill was not fully identified (Scaife et al. 2014; Kang et al. 2014; Riddle et al. 2013; Butler et al. 2016). Some studies suggested that the stratosphere plays a role in Northern Hemisphere winter climate variability using simulations from an atmospheric general circulation model (AGCM; Scaife et al. 2005; Douville 2009). Douville (2009), for example, quantified the stratospheric contribution on the interannual variability of winter surface air temperature and precipitation over the Northern Hemisphere in AGCM simulations in which the stratosphere was relaxed to observations. However, in real-time seasonal predictions, whether such variability driven by the stratosphere is predictable has not been fully addressed. The present study not only identifies the stratospheric-driven variability in model simulations but also further reveals the stratospheric influence on predictive skill in an operational seasonal forecasting system. A few other studies showed seasonal predictive skill of the NAO and surface climate arising from the stratosphere in climate forecasting systems under extreme stratospheric conditions (Scaife and Knight 2008; Stockdale et al. 2015; Tripathi et al. 2015; Scaife et al. 2016; Fereday et al. 2012; Sigmond et al. 2013; Domeisen et al. 2015). However, separating the general role of the stratosphere in seasonal predictive skill of surface climate is very challenging because of the strong coupling between the stratosphere and troposphere. In this study, we set up a suite of numerical experiments, including both climate simulations and retrospective forecasts, to isolate the role of the stratosphere in seasonal predictive skill of the Northern Hemisphere extratropical surface climate. The results clearly reveal the actual predictive skill driven by the stratosphere in a coupled real-time forecasting system and prove the fundamental mechanism connecting the stratosphere and troposphere in both observations and model predictions.

2. Model, experiments, data, and method

a. Model description

The Geophysical Fluid Dynamics Laboratory (GFDL) high-resolution Forecast-Oriented Low Ocean Resolution (FLOR) model is used in this study (Vecchi et al. 2014). FLOR is a new coupled global climate model developed based on the GFDL Climate Model, version 2.5, (CM2.5; Delworth et al. 2012) and Climate Model, version 2.1, (CM2.1; Delworth et al. 2006). It has a horizontal resolution of 50 (100) km, and 32 (50) vertical levels in the atmosphere (ocean). The upper boundary is 1 hPa. FLOR is used in real-time seasonal predictions, contributing to the North American Multimodel Ensemble (NMME) for seasonal prediction (Kirtman et al. 2014). An additional description of FLOR can be found in Vecchi et al. (2014).

b. Experiments

We conducted two sets of experiments consisting of two constrained simulation experiments and three retrospective forecast experiments using FLOR, and the two sets of experiments are summarized in Tables 1 and 2. These experiments are used to isolate the role of the stratosphere in seasonal prediction of surface climate.

1) FLOR CONSTRAINED EXPERIMENTS

The first set of experiments consists of two constrained simulation experiments, simulating the climate

TABLE 2. List of FLOR retrospective forecast experiments.

Expt name	Atmospheric/land initial conditions	Ocean/sea ice initial conditions	Radiative forcing	Time period	Ensemble size
SST-forcedAIC	AM2.5 forced by observed SST	Ensemble Coupled Data Assimilation	Time varying	1981–2015	12
ObsSIC	Horizontal winds and temperatures above 100 hPa relaxed to MERRA (6-h time scale)	Ensemble Coupled Data Assimilation	Time varying	1981–2015	12
ObsAIC	Surface pressure, horizontal winds, and temperatures of entire atmosphere column relaxed to MERRA (6-h time scale)	Ensemble Coupled Data Assimilation	Time varying	1981–2015	12

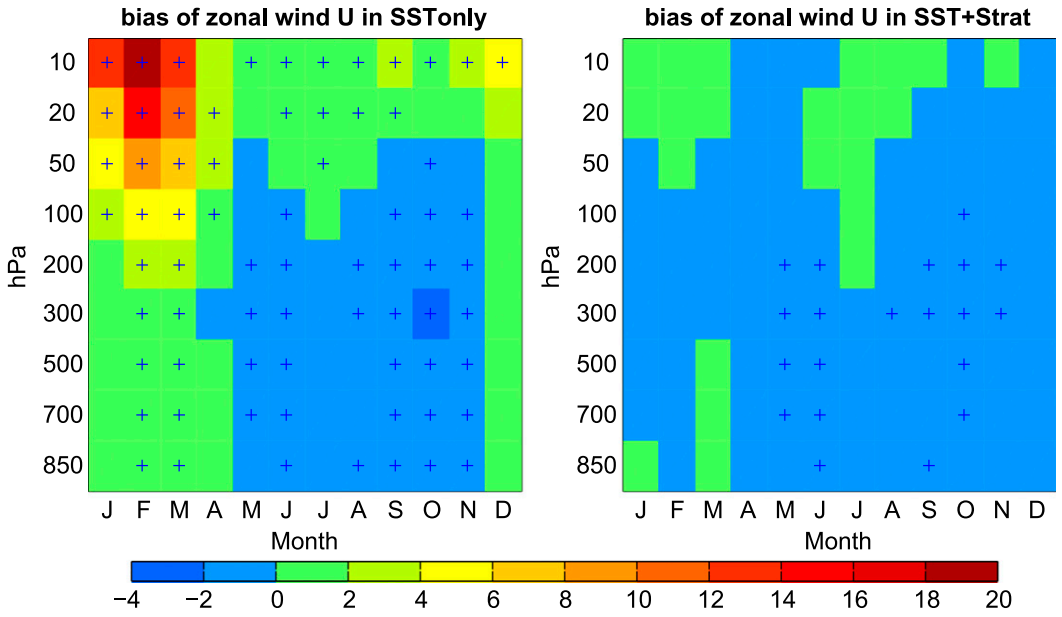

FIG. 1. Climatological bias of zonal mean zonal wind (m s^{-1}) averaged over 60°–90°N as a function of month and pressure level in the ensemble mean simulations from (left) SSTonly and (right) SST+Strat. The verification data used here are the zonal wind from MERRA from 1981 to 2015. The cross symbol indicates the bias is significant at the 5% level based on a *t* test.

from 1981 to 2015. Each experiment contains five ensemble members. In the first experiment, the time-varying SSTs are relaxed to the observations from HadISST1 (Rayner et al. 2003) on a 5-day time scale (called the SSTonly simulation). In the second experiment, the relaxation of SSTs is identical to SSTonly; in addition, the horizontal winds and temperatures in the stratosphere (above 100 hPa) are relaxed to the Modern-Era Retrospective Analysis for Research and Applications (MERRA; Rienecker et al. 2011) on a 6-h time scale with a tapering factor α (called the SST+Strat simulation). The tapering factor α is one for model layers above 50 hPa (i.e., 1, 4, 8, 14, 21, 30, and 41 hPa) and is zero for model layers below 100 hPa. From 50 to 100 hPa, α is linearly reduced from one to zero, allowing a smooth transition from the stratosphere to troposphere. Figure 1 shows the climatological bias of zonal mean zonal wind averaged over 60°–90°N as a function of month and pressure level for SST+Strat and SSTonly. In SSTonly, large positive bias is seen in the stratosphere (i.e., the polar vortex is too strong), particularly in the boreal winter season from January to March. The stratospheric bias in SST+Strat is considerably reduced compared to SSTonly because of the relaxation of stratospheric variables to the observed information in SST+Strat. The radiative forcings in these two experiments are based on observational estimates before 2005 and projections of the representative concentration pathways scenario 4.5 (RCP4.5; Meinshausen et al. 2011) after 2005. Details of these two FLOR constrained experiments are listed in Table 1.

2) FLOR RETROSPECTIVE FORECASTS

The second set of experiments consists of three retrospective ensemble forecast experiments. In the first forecast experiment, the atmospheric and land initial conditions are taken from ensemble simulations of the atmospheric component of FLOR [the GFDL Atmospheric Model, version 2.5 (AM2.5)] that is forced by observed SST, called SST-forcedAIC. The atmospheric and land initial conditions in the second experiment are from a set of relaxation-toward-observation coupled FLOR simulations in which the stratospheric (above 100 hPa) temperatures and horizontal winds are relaxed toward MERRA on a 6-h time scale, as detailed above (hereinafter ObsSIC). Since ObsSIC includes observed initial conditions only in the stratosphere, it does not contain tropospheric weather information. The third forecast experiment is conducted with an identical configuration to ObsSIC, except that the atmospheric and land initial conditions are from a set of FLOR simulations in which the surface pressure, horizontal winds, and temperatures throughout the entire atmosphere are relaxed toward MERRA on a 6-h time scale (hereinafter ObsAIC; Jia et al. 2016; X. Yang et al. 2016, unpublished manuscript). The ocean and sea ice initial conditions in these three retrospective forecasts are identical and are from GFDL's Ensemble Coupled Data Assimilation (ECDA)

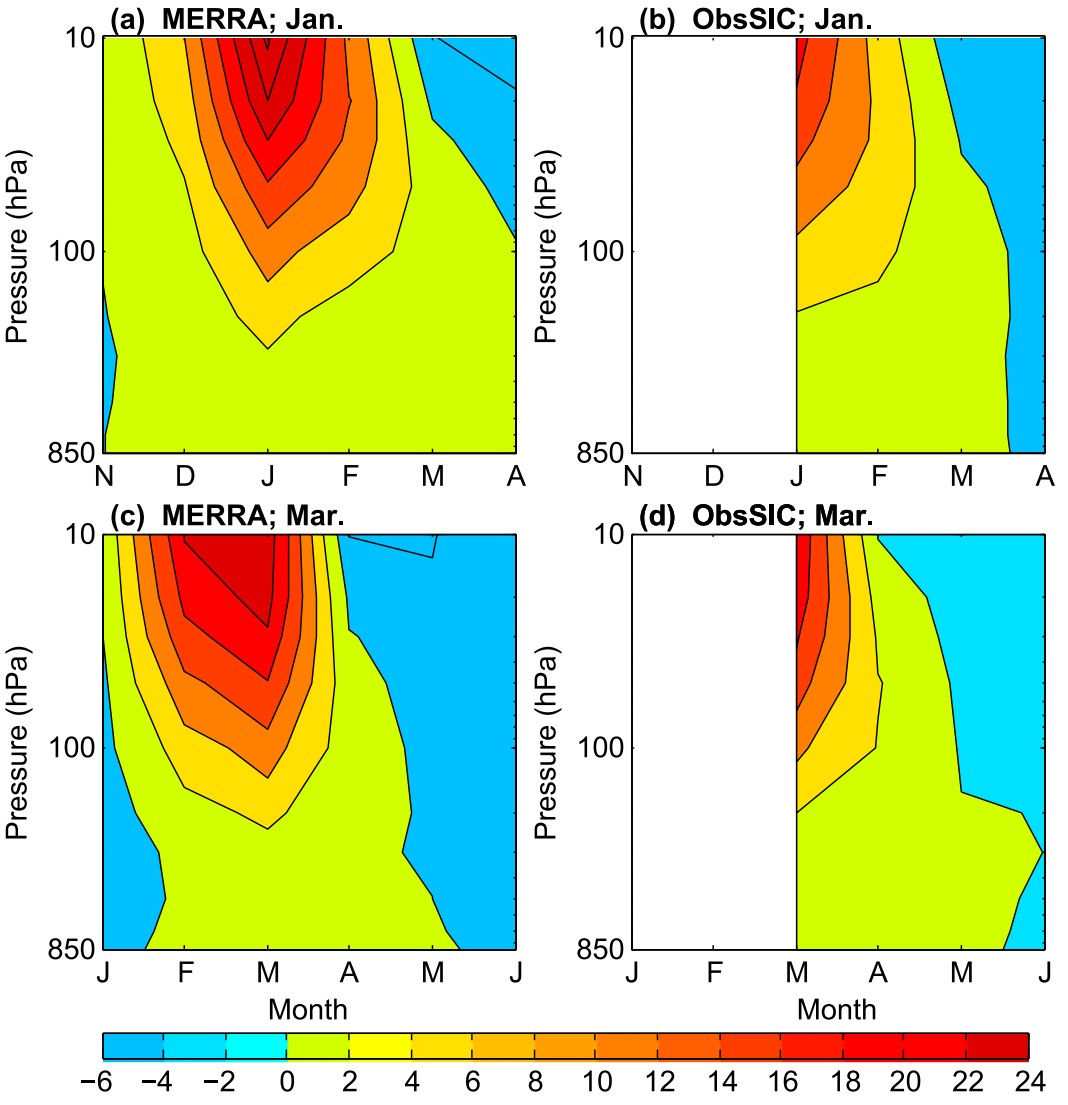

FIG. 2. Time–height evolution of the zonal mean zonal wind (averaged over 60°–90°N) composite differences ($m\,s^{-1}$) between the 5 years with strongest zonal mean zonal wind and the 5 years with weakest zonal mean zonal wind at 50 hPa in (top) January and (bottom) March for (left) MERRA and (right) model predictions from ObsSIC. The model predictions are initialized on (b) 1 Jan and (d) 1 Mar; thus, results are not available prior to the initialization date.

system designed for CM2.1 (Zhang et al. 2007). The radiative forcings in these three experiments are identical to those in the FLOR constrained experiments described above. Each retrospective forecast experiment contains 12 ensemble members. Each ensemble member is initialized on the first date of each month and integrated for 12 months. The retrospective forecasts during 1981–2015 are analyzed in this study. Details on these three retrospective forecast experiments are displayed in Table 2.

c. *Observational data*

The observed near-surface (2 m) temperatures were from the Climatic Research Unit Time Series, version 3.10 (CRU TS v. 3.10) at a 0.5° resolution (Harris et al. 2014). The observed Niño-3.4 index was downloaded from the National Oceanic and Atmospheric Administration's website (http://www.cpc.ncep.noaa.gov/data/indices/ersst3b.nino.mth.81-10.ascii). We also used zonal wind and sea level pressure (SLP) from MERRA products.

d. *Method*

To isolate predictable patterns of sea level pressure, we use the signal-to-noise maximizing empirical orthogonal function (S/N EOF) method, which optimizes the ratio of signal-to-noise variance. This method,

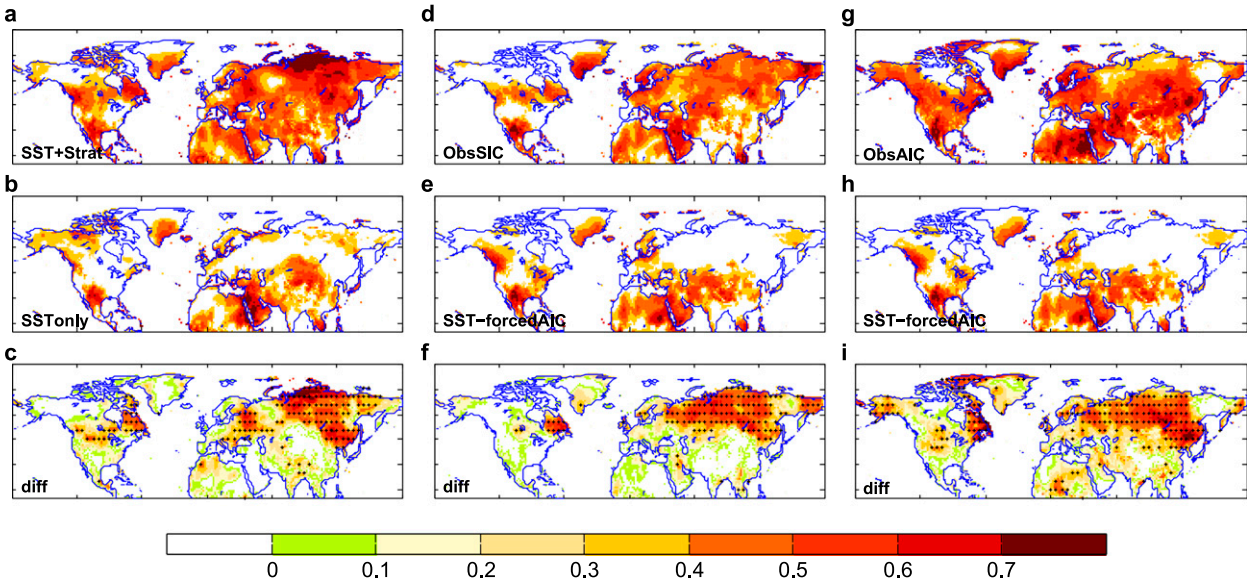

FIG. 3. The point-by-point correlation skill of boreal spring (MAM) near-surface (2 m) land temperature in (a) SST+Strat, (b) SSTonly, (c) SST+Strat − SSTonly, (d) ObsSIC, (e) SST-forcedAIC, (f) ObsSIC − SST-forcedAIC, (g) ObsAIC, (h) SST-forcedAIC, and (i) ObsAIC − SST-forcedAIC. The retrospective forecasts from ObsSIC, ObsAIC, and SST-forcedAIC are initialized on 1 Mar. Results are from 12-member means for ObsSIC, ObsAIC, and SST-forcedAIC and 5-member means for SSTonly and SST+Strat. Insignificant (5% level) areas are masked out in (a),(b),(d),(e),(g), and (h). The stippling in (c),(f), and (i) indicates the difference in correlation skill is significant at the 10% level. The verification data used here are the 2-m temperature from the CRU during 1981–2014.

developed by Allen and Smith (1997), has been widely used in previous studies, including ones on climate change and climate predictability, to extract the S/N EOF patterns (Venzke et al. 1999; Chang et al. 2000; Hu and Huang 2007; Ting et al. 2009; DelSole et al. 2011). In the context of ensemble simulations, the ''signal'' is estimated as the ensemble mean over all ensemble members, representing the consistency among ensemble members. The ''noise'' is estimated as the distance from the ensemble mean. This method produces an ordered set of patterns such that the first maximizes the ratio of signal-to-noise variance, the second maximizes this ratio subject to being uncorrelated with the first, and so on.

3. Results

The stratosphere–troposphere coupling is the strongest during the boreal winter season, when the planetary waves from the troposphere propagate upward into the stratosphere. As a consequence, the stratospheric polar vortex and the westerly winds are weakened. The stratospheric wind anomalies migrate downward, affecting surface climate (Baldwin and Dunkerton 2001; Kidston et al. 2015). Figures 2a and 2b show the time–height evolution of the zonal mean zonal wind (averaged over 60°–90°N) composite differences between the 5 years with strongest zonal mean zonal wind and the 5 years with weakest zonal mean zonal wind at 50 hPa in January. The wind anomalies in the stratosphere, peaking in January, extend to the troposphere in March and April in MERRA and model predictions from ObsSIC. Similar features are found for the composites derived based on the zonal mean zonal wind in March (Figs. 2c,d): that is, the strongest wind anomalies in March are able to influence the troposphere until May. Although the largest stratospheric variability occurs in winter, the stratospheric variations in winter and early spring influence the seasonal mean surface climate in the spring season, primarily because of the delayed impacts from the stratosphere to the troposphere (Baldwin and Dunkerton 1999, 2001). In this study, we explore the role of the stratosphere in surface prediction in both winter [January–March (JFM)] and spring [March–May (MAM)] seasons. Surprisingly, given the known strong troposphere–stratosphere coupling during winter, we find that the predictive skill of near-surface land temperature driven by the stratosphere is lower in JFM than MAM in the FLOR forecasting system (section 3d), presumably partly because of the strong stratospheric bias in JFM season in FLOR. More discussions on the results for the JFM and MAM seasons are provided below.

a. Predictive skill of near-surface land temperature in MAM

We first evaluate the stratospheric impact on the variability of Northern Hemisphere near-surface (at 2 m) land temperature in MAM from the two constrained

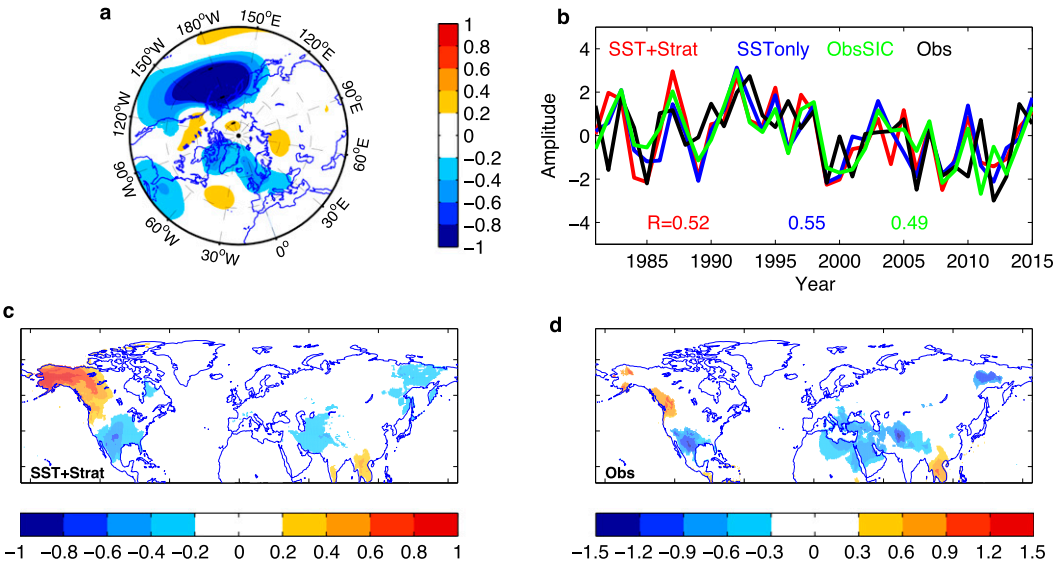

FIG. 4. (a) The first potentially predictable pattern of MAM mean SLP (hPa) in SST+Strat simulations. (b) The ensemble mean time series associated with the predictable SLP pattern in SST+Strat, SSTonly, ObsSIC, and the observations. The regression map of near-surface land temperature (c) with the predictable SLP pattern in SST+Strat, and (d) from CRU observations with the observed Niño-3.4 index. The MAM SLP in ObsSIC is initialized on 1 Mar. The values in (b) are the anomaly correlation coefficients between the time series in SST+Strat (red), SSTonly (blue), ObsSIC (green), and the observations (black). Insignificant areas (at the 10% level) are masked out in (c) and (d).

simulation experiments (i.e., SSTonly and SST+Strat). Recall that SST+Strat has additional observed stratospheric information relative to SSTonly; hence, improvement in the simulation of temperature in SST+Strat is attributable to the stratosphere. Figures 3a and 3b show the point-by-point temporal correlations of temperature between the observed and ensemble mean anomalies from SST+Strat and SSTonly. Compared to SSTonly, SST+Strat shows significantly higher correlations over the extratropics, particularly over northern Eurasia and northern North America (Fig. 3c). These results reveal the stratospheric impact on the interannual variability of near-surface land temperature over Northern Hemisphere extratropics, consistent with the results in Douville (2009).

However, the additional correlation skill gained in SST+Strat is estimated given realistic stratospheric information. In other words, it is the potential (upper limit of) predictability, assuming one is able to predict the stratosphere perfectly. In the forecasting system, a realistic stratosphere is only given at the initial state, and the stratosphere cannot be predicted perfectly. Therefore, the predictions made from the forecasting system may not be able to realize the potential predictability estimated from the simulations with observed stratospheric information. A question we ask is whether the potential predictability driven by the stratosphere can be realized in the real-time forecasting system. To address this question, we investigate the predictive skill of seasonal mean temperature in FLOR retrospective forecast experiments: SST-forcedAIC and ObsSIC. As shown in Fig. 3d, the MAM near-surface land temperature in most areas over the Northern Hemisphere can be predicted with significant skill in ObsSIC, which contains additional observed information in the stratospheric initial conditions relative to SST-forcedAIC. Most importantly, the correlation skill in ObsSIC is substantially higher than the skill in SST-forcedAIC (Fig. 3e) over northern Eurasia and northeastern North America. The above results reveal that the stratospheric-driven potential predictability over extratropics can be predicted skillfully in the FLOR forecasting system. The large-scale structure of the actual predictive skill driven by the stratosphere (Fig. 3f) is consistent with the potential skill arising from the stratosphere estimated from the constrained simulations (Fig. 3c). Sigmond et al. (2013) and Tripathi et al. (2015) also documented enhanced forecast skill of wintertime surface temperature over northern Russia and eastern Canada when initializing the stratosphere during sudden warmings, which is in line with our results. Note that the above predictive skill of MAM temperature in ObsSIC and SST-forcedAIC is computed using predictions initialized on 1 March, which are considered as lead-0-month predictions for MAM. We also investigate the predictions of MAM temperature initialized on 1 February (i.e., lead-1-month predictions for MAM) in ObsSIC

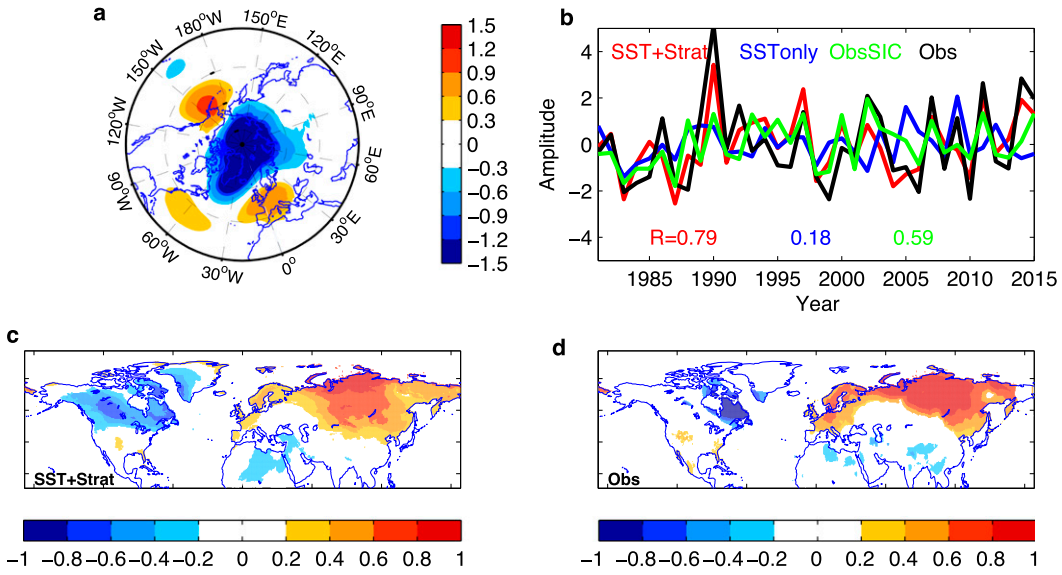

FIG. 5. As in Fig. 4, but for the second potentially predictable pattern. In (d) the regression is performed with the AO index derived from MERRA.

and SST-forcedAIC and find the skill levels in the two experiments are comparable (figure not shown). There is no significantly higher skill in ObsSIC than SST-forcedAIC for lead-1-month predictions. This is expected because the seasonal mean stratospheric variability is generally unpredictable a month ahead in this model. Thus, lead-0-month predictions initialized with observed stratospheric information may be better able to predict stratospheric influence on surface climate.

We now further investigate the predictive skill in ObsAIC. Compared to ObsSIC, ObsAIC includes additional observed initial conditions in the troposphere. As seen from Figs. 3f and 3i, ObsAIC shows slightly higher skill than ObsSIC in places such as Alaska, central Canada, and central Europe, implying the tropospheric initial conditions play a certain role in the predictive skill of surface temperature. In addition, relative to SST-forcedAIC, ObsAIC also shows enhanced skill over northern Eurasia and northeastern North America (Fig. 3i), similar to the results from experiments with observed stratospheric initial conditions (Figs. 3c,f). This again suggests that the stratosphere is the primary source of the enhanced skill over northern Eurasia and northeastern North America.

Note that the 0-lead seasonal predictive skill derived from ObsAIC includes the weather skill in the first week or so. However, this is not the case for ObsSIC. In the initial conditions of ObsSIC, the day-to-day weather states are not in phase with those in the observations (figure not shown), but the low-frequency variations like the AO are correlated with observed ones (see Fig. 5). Thus, the contribution of weather skill to the 0-lead seasonal prediction is ruled out in ObsSIC. We therefore directly demonstrate that the dominant predictability source of 0-lead seasonal prediction is not from the predictable extratropical weather patterns in the first week or so.

b. *Potentially predictable pattern of sea level pressure in MAM*

To understand the mechanism that leads to the improved skill of near-surface land temperature in SST+Strat, ObsSIC, and ObsAIC, we identify potentially predictable patterns of MAM mean SLP over 20°–90°N in the SST+Strat simulations using the S/N EOF method and then project the predictable patterns onto other experiments and the observations to obtain their associated temporal variations.

The most potentially predictable pattern shows the extratropical teleconnection associated with El Niño, with the largest negative SLP anomalies over the northern Pacific (Fig. 4a). The regression map of near-surface land temperature (Fig. 4c) on this pattern displays an El Niño–related structure and is similar to the regression pattern of temperature on the Niño-3.4 index in the observations (Fig. 4d). The time series of this pattern in SST+Strat, SSTonly, ObsSIC, and the observations are all significantly correlated with the observed Niño-3.4 index, suggesting that the source of the skill arises from the ocean (Fig. 4b). This argument is also supported by the comparable correlation skill between the time series in the observations and the time series in SST+Strat ($R = 0.52$) and SSTonly ($R = 0.55$), because both of these two simulation experiments contain predictability from the SSTs. Moreover, this pattern is highly predictable in ObsSIC predictions with a

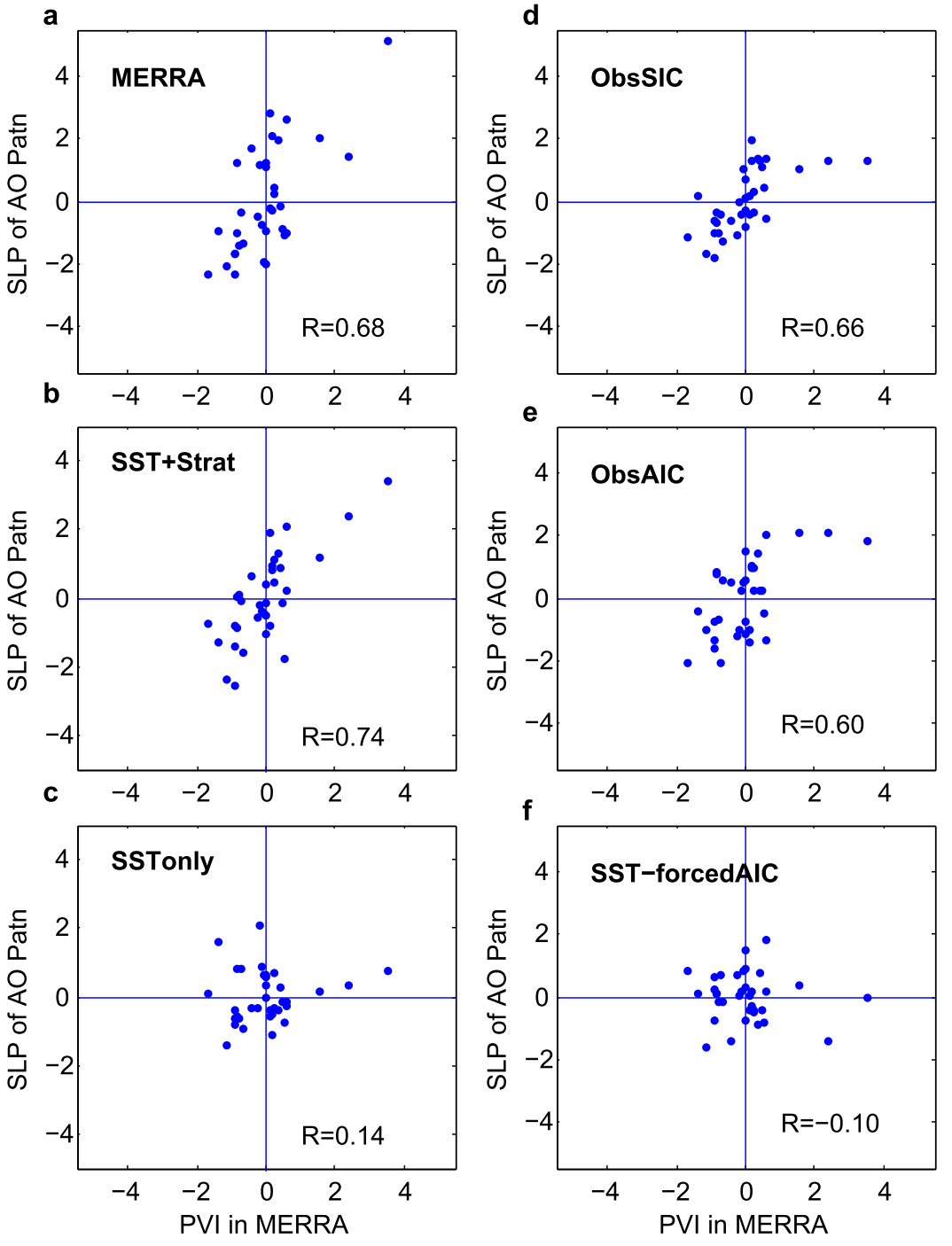

FIG. 6. Scatterplot of the MAM mean normalized polar vortex index derived from MERRA vs the time series of the MAM mean SLP anomalies of the second potentially predictable pattern (i.e., the AO pattern in Fig. 5a) in (a) MERRA, and ensemble mean of (b) SST+Strat, (c) SSTonly, (d) ObsSIC, (e) ObsAIC, and (f) SST-forcedAIC.

significant correlation skill of 0.62, comparable to the skill shown in other forecast models (Athanasiadis et al. 2014).

In contrast to the oceanic forcing of the first predictable pattern, the second potentially predictable pattern is primarily driven by the stratosphere. This pattern shows an AO structure. The largest negative SLP anomalies are found over the polar region and positive anomalies are found over the extratropics (Fig. 5a). Unlike the ensemble mean time series of this pattern in SST+Strat, which is significantly correlated with the observed time series

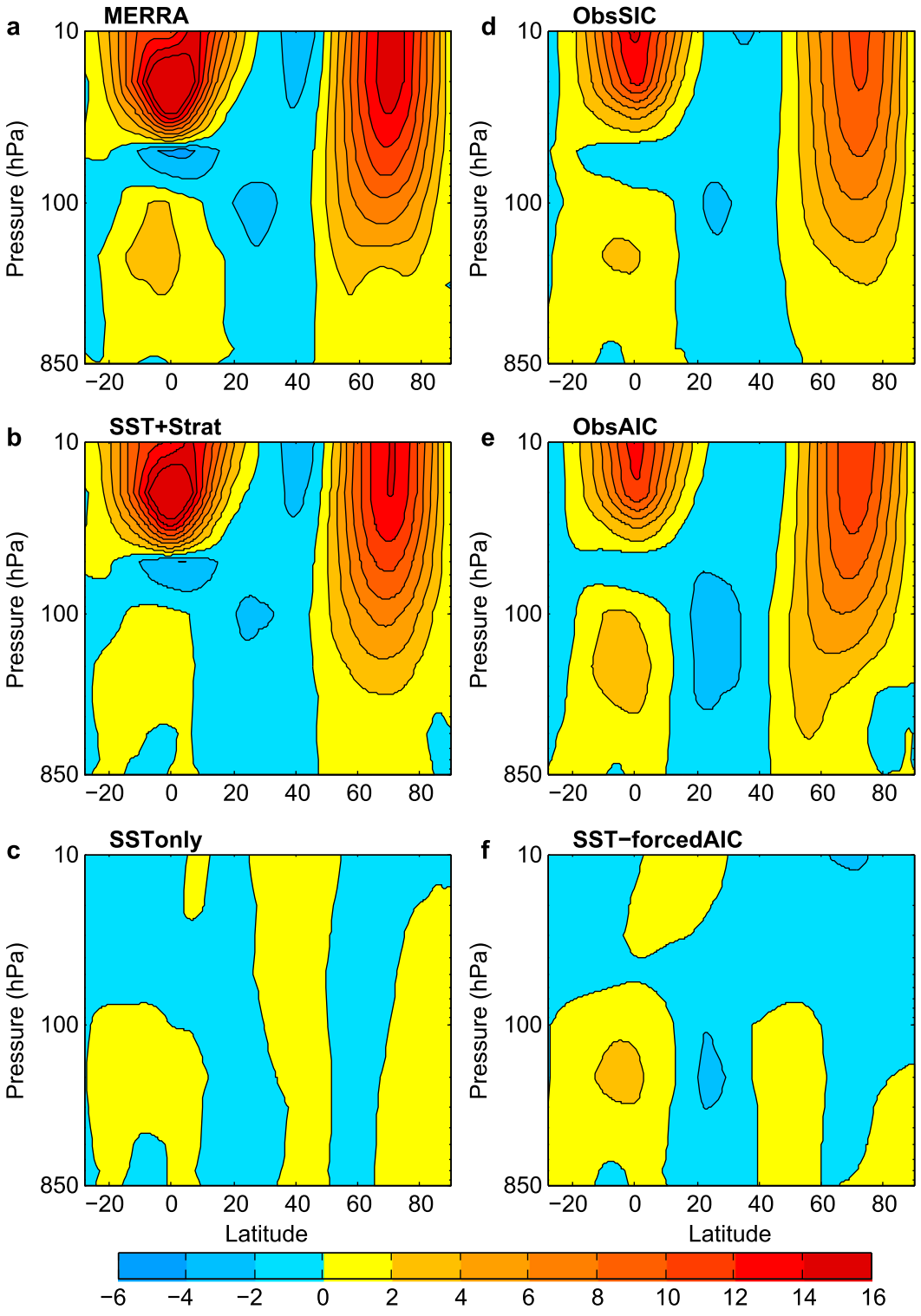

FIG. 7. The composite differences of MAM zonal mean zonal wind between the 5 years with strongest polar vortex and the 5 years with the weakest polar vortex in (a) MERRA, and ensemble mean of (b) SST+Strat, (c) SSTonly, (d) ObsSIC, (e) ObsAIC, and (f) SST-forcedAIC. The polar vortex is derived based on the zonal mean zonal wind averaged over 60°–90°N at 50 hPa from MERRA.

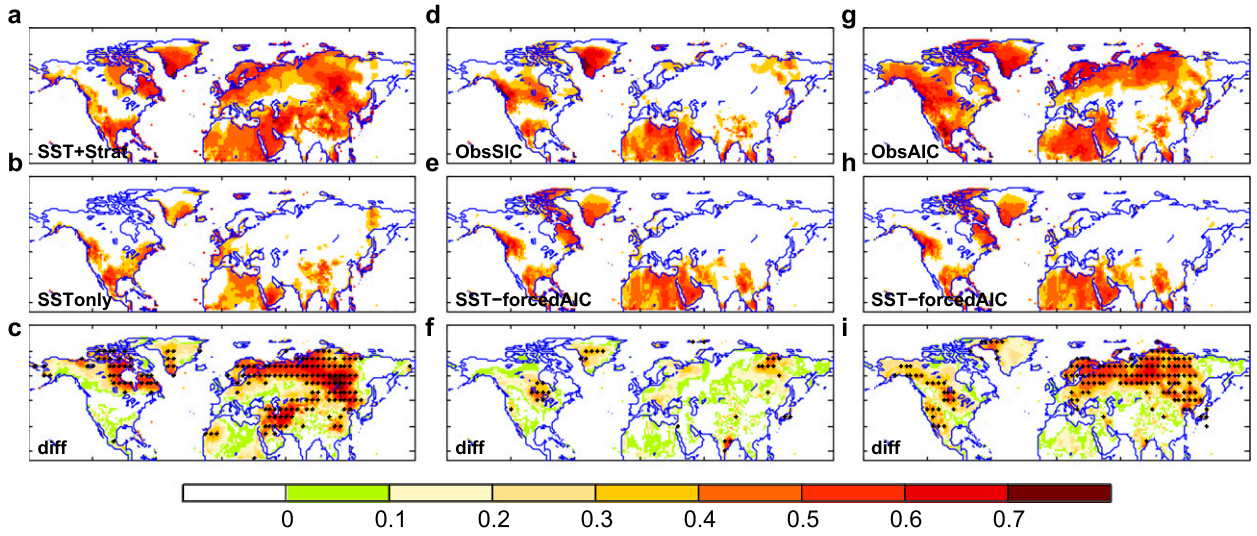

FIG. 8. As in Fig. 3, but for the JFM season.

($R = 0.79$), the ensemble mean time series in SSTonly is unable to capture the observed evolution of the pattern ($R = 0.18$). We thus claim that the stratosphere is the key predictability source of the AO pattern (Fig. 5b). Strikingly, this AO pattern is skillfully predicted ($R = 0.59$) in FLOR seasonal forecasts with observed stratospheric initial conditions (i.e., ObsSIC).

The regression map of the near-surface land temperature on the AO pattern in SST+Strat (Fig. 5c) resembles the observed AO teleconnection pattern (Fig. 5d). The largest amplitudes are shown over northern Eurasia and northern North America, where skillful surface temperature predictions driven by the stratosphere are found (Fig. 3). The above results suggest that the improved skill in extratropical land temperature is associated with the AO and is primarily driven by the stratosphere.

c. *Dynamical connection between the stratosphere and troposphere in MAM*

The dynamical connection between surface climate and the stratosphere is demonstrated in the scatterplot between the normalized stratospheric polar vortex index (PVI) from MERRA and SLP anomalies of the AO pattern in MERRA, two constrained simulations, and three retrospective forecast experiments (Fig. 6). Here, the PVI is defined as the zonal mean zonal wind at 50 hPa averaged over 60°–90°N. Significant correlation between the observed PVI and SLP anomalies of the AO pattern is found in MERRA and in the experiments including the observed stratospheric information (i.e., SST+Strat, ObsSIC, and ObsAIC). In contrast, there is no significant relationship between the observed PVI and the simulated SLP anomalies in the experiments without realistic stratospheric state (i.e., SSTonly and SST-forcedAIC).

Further evidence of the dynamical connection between the stratosphere and troposphere is shown in the zonal mean zonal wind composite differences between the 5 years with strongest PVI and the 5 years with weakest PVI (Fig. 7). These 10 extreme stratospheric polar vortex years are chosen based on MERRA. As seen from Fig. 7a, the strong extratropical stratospheric westerlies, north of around 50°N, extend to the lower troposphere, which provides the dynamical condition for the impact of the stratosphere on the troposphere. This feature is well captured in the ensemble mean SST+Strat simulations (Fig. 7b). We emphasize that such a connection is reproduced in ObsSIC and ObsAIC predictions with stratosphere initialization (Figs. 7d,e), again highlighting the role of the stratosphere in seasonal prediction of surface climate. Consistent with the results shown in Fig. 6, the SSTonly and SST-forcedAIC experiments do not show connection between the stratosphere and troposphere.

d. *Predictive skill of near-surface land temperature in JFM*

In this section, we discuss the results for the boreal winter season. In summary, we repeat the above calculations for JFM. We find, in general, the skill is lower in JFM than MAM in all experiments, particularly in ObsSIC. The stratospheric-driven potential predictability estimated in relaxation-toward-observation simulations is not achieved in the predictions with stratosphere initialization (i.e., ObsSIC), but it is well realized in the predictions with initialization of the entire atmosphere (i.e., ObsAIC). Possible reasons for the low predictive skill in JFM are discussed below.

Figure 8 displays the point-by-point correlation skill of JFM near-surface land temperature in FLOR

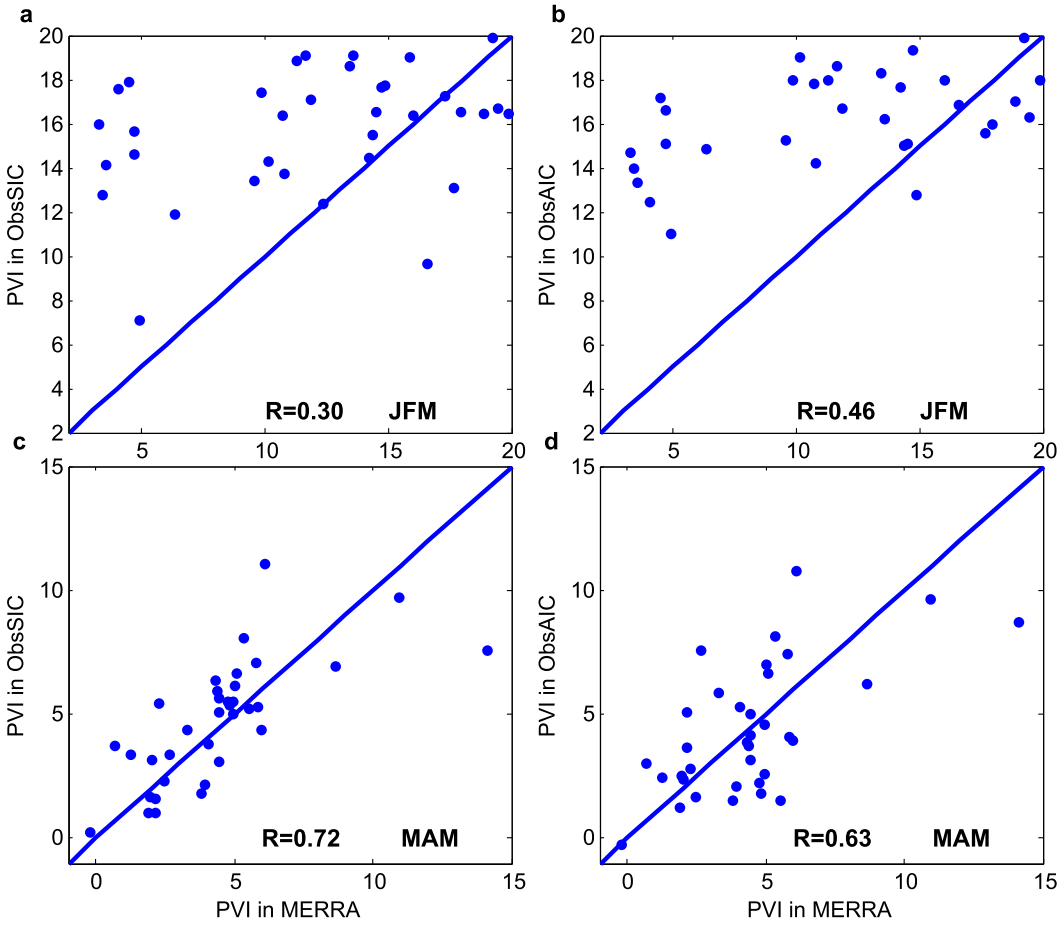

FIG. 9. Scatterplot between the PVI in MERRA and the PVI in (left) ObsSIC and (right) ObsAIC for (top) JFM and (bottom) MAM seasons. The value in each panel indicates the correlation coefficient between the PVI in MERRA and the PVI in predictions.

simulation experiments and retrospective forecast experiments. Similar to the MAM season, the ensemble simulations with realistic stratosphere (i.e., SST+Strat) demonstrate higher skill over northeastern North America and northern Eurasia relative to the simulations without realistic stratosphere (i.e., SSTonly). However, unlike the results for the MAM season, the potential predictability driven by the stratosphere is not achieved in ObsSIC (Fig. 8d). Only limited areas show significantly higher skill in ObsSIC than SST-forcedAIC (Fig. 8f). But, including additional observed tropospheric initial conditions, the ObsAIC experiment does show higher predictive skill over North America and northern Eurasia than SST-forcedAIC (Fig. 8i).

To understand why the winter potential predictability driven by the stratosphere is not well predicted in ObsSIC, we show in Figs. 9a and 9c the scatterplots between the PVI derived from MERRA and the PVI in ObsSIC for JFM and MAM seasons. In JFM, ObsSIC tends to overestimate the PVI, particularly for the weak polar vortex years. In contrast to the winter season, the observed PVI in spring is well predicted in ObsSIC ($R = 0.72$), although the polar vortices are weaker in spring than in winter. The overestimation of the PVI in JFM may be a result of the large stratospheric wind bias in FLOR for winter season, as shown in Fig. 1. Because of the positive stratospheric wind bias, FLOR fails to predict weak polar vortices, resulting in limited skill in predicting surface climate over the extratropics. Interestingly, adding realistic tropospheric initial conditions, the correlation between the PVI in MERRA and in ObsAIC is higher in JFM but lower in MAM than the correlation in ObsSIC (Figs. 9b,d). This indicates the tropospheric conditions play a certain role in the forecast of the polar vortex in winter, supporting the fact that the stratosphere–troposphere coupling is strong in winter. However, for the spring season, the downward influence from the stratosphere to the troposphere may dominate. The strong coupling between the stratosphere and

troposphere in the winter season might also lead to low skill in the prediction of surface climate.

4. Summary and discussion

This study explores the role of the stratosphere in seasonal prediction of extratropical near-surface land temperature in boreal winter (JFM) and spring (MAM) seasons. We design two sets of target experiments using FLOR to isolate the role of the stratosphere. One set of experiments consists of two constrained simulation experiments with and without the observed stratospheric state. The other set of retrospective forecast experiments consists of ensemble predictions with and without observed stratospheric initial conditions and ensemble predictions with observed initial conditions in both the stratosphere and troposphere. Using these experiments, we reveal that the stratosphere is the driver of skillful seasonal prediction of near-surface land temperature over the extratropics, particularly over northern Eurasia for the MAM season. The stratosphere affects surface climate through its influence on the AO. The dynamical connection between the stratosphere and the troposphere in the observations and model predictions is demonstrated by the significant correlations between the stratospheric PVI and SLP anomalies, as well as the migration of stratospheric zonal wind anomalies to the lower troposphere. As for the JFM season, the potential predictability driven by the stratosphere is not well achieved in the FLOR retrospective forecast experiment that has observed stratospheric initial conditions (i.e., ObsSIC), presumably because of the strong positive stratospheric wind bias in the JFM season in FLOR. ObsSIC fails to predict weak polar vortices, thus adding little skill relative to the predictions without realistic stratospheric initial conditions (i.e., SST-forcedAIC). In addition, the strong coupling between the stratosphere and troposphere in the winter season (JFM) might lead to low skill in the prediction of surface climate.

We emphasize the connection between the stratosphere and surface climate on seasonal time scales because the stratosphere influences surface climate through modulating large-scale circulation (e.g., AO) on seasonal scales. Presumably because of the strong stratospheric zonal wind bias in the JFM season, FLOR tends to underestimate weak polar vortices. With the development of climate models that better represent the stratosphere dynamics and the stratosphere–troposphere coupling, the predictive skill of Northern Hemisphere extratropical surface climate in winter is expected to be improved. This study provides a scientific basis for model development. Our results also have practical implications for climate services, including for instance sectors and the transport system (Palin et al. 2016).

Acknowledgments. The authors thank three anonymous reviewers for insightful comments that helped to improve this manuscript. We also thank Drs. Vaishali Naik and Karin van der Wiel at GFDL for constructive comments on an earlier draft of this manuscript. This research was supported by the NOAA's Climate Program Office. Drs. G. Vecchi and X. Yang were supported by NOAA/OAR under the auspices of the National Earth System Prediction Capability (National ESPC). Prof. Scaife was supported by the Joint DECC/Defra Met Office Hadley Centre Climate Programme (GA01101) and the EU FP7 SPECS project.

REFERENCES

Allen, M. R., and L. A. Smith, 1997: Optimal filtering in singular spectrum analysis. *Phys. Lett.*, **234**, 419–428, doi:10.1016/S0375-9601(97)00559-8.

Athanasiadis, P. J., and Coauthors, 2014: The representation of atmospheric blocking and the associated low-frequency variability in two seasonal prediction systems. *J. Climate*, **27**, 9082–9100, doi:10.1175/JCLI-D-14-00291.1.

Baldwin, M. P., and T. J. Dunkerton, 1999: Propagation of the Arctic Oscillation from the stratosphere to the troposphere. *J Geophys. Res.*, **104**, 30 937–30 946, doi:10.1029/1999JD900445.

——, and ——, 2001: Stratospheric harbingers of anomalous weather regimes. *Science*, **294**, 581–584, doi:10.1126/science.1063315.

——, D. B. Stephenson, D. W. J. Thompson, T. J. Dunkerton, A. J. Charlton, and A. O'Neill, 2003: Stratospheric memory and skill of extended-range weather forecasts. *Science*, **301**, 636–640, doi:10.1126/science.1087143.

Butler, A. H., and Coauthors, 2016: The Climate-System Historical Forecast Project: Do stratosphere-resolving models make better seasonal climate predictions in boreal winter? *Quart. J. Roy. Meteor. Soc.*, **142**, 1413–1427, doi:10.1002/qj.2743.

Chang, P., R. Saravanan, L. Ji, and G. C. Hegerl, 2000: The effect of local sea surface temperatures on atmospheric circulation over the tropical Atlantic sector. *J. Climate*, **13**, 2195–2216, doi:10.1175/1520-0442(2000)013<2195:TEOLSS>2.0.CO;2.

Cohen, J., M. Barlow, P. J. Kushner, and K. Saito, 2007: Stratosphere–troposphere coupling and links with Eurasian land surface variability. *J. Climate*, **20**, 5335–5343, doi:10.1175/2007JCLI1725.1.

DelSole, T., M. K. Tippett, and J. Shukla, 2011: A significant component of unforced multidecadal variability in the recent acceleration of global warming. *J. Climate*, **24**, 909–926, doi:10.1175/2010JCLI3659.1.

Delworth, T. L., and Coauthors, 2006: GFDL's CM2 global coupled climate models. Part I: Formulation and simulation characteristics. *J. Climate*, **19**, 643–674, doi:10.1175/JCLI3629.1.

——, and Coauthors, 2012: Simulated climate and climate change in the GFDL CM2.5 high-resolution coupled climate model. *J. Climate*, **25**, 2755–2781, doi:10.1175/JCLI-D-11-00316.1.

Domeisen, D., A. H. Butler, K. Fröhlich, M. Bittner, W. A. Müller, and J. Baehr, 2015: Seasonal predictability over Europe arising from El Niño and stratospheric variability in the MPI-ESM seasonal prediction system. *J. Climate*, **28**, 256–271, doi:10.1175/JCLI–D–14–00207.1.

Douville, H., 2009: Stratospheric polar vortex influence on Northern Hemisphere winter climate variability. *Geophys. Res. Lett.*, **36**, L18703, doi:10.1029/2009GL039334.

Fereday, D. R., A. Maidens, A. Arribas, A. A. Scaife, and J. R. Knight, 2012: Seasonal forecasts of Northern Hemisphere winter 2009/10. *Environ. Res. Lett.*, **7**, 034031, doi:10.1088/1748-9326/7/3/034031.

Harris, I., P. D. Jones, T. J. Osborn, and D. H. Lister, 2014: Updated high-resolution grids of monthly climatic observations—The CRU TS3.10 dataset. *Int. J. Climatol.*, **34**, 623–642, doi:10.1002/joc.3711.

Hu, Z., and B. Huang, 2007: The predictive skill and the most predictable pattern in the tropical Atlantic: The effect of ENSO. *Mon. Wea. Rev.*, **135**, 1786–1806, doi:10.1175/MWR3393.1.

Jia, L., X. Yang, G. A. Vecchi, R. G. Gudgel, T. Delworth, and A. Rosati, 2015: Improved seasonal prediction of temperature and precipitation over land in a high-resolution GFDL climate model. *J. Climate*, **28**, 2044–2062, doi:10.1175/JCLI-D-14-00112.1.

——, and Coauthors, 2016: The roles of radiative forcing, sea surface temperatures, and atmospheric and land initial conditions in U.S. summer warming episodes. *J. Climate*, **29**, 4121–4135, doi:10.1175/JCLI-D-15-0471.1.

Kang, D., and Coauthors, 2014: Prediction of the Arctic Oscillation in boreal winter by dynamical seasonal forecasting systems. *Geophys. Res. Lett.*, **41**, 3577–3585, doi:10.1002/2014GL060011.

Kidston, J., A. A. Scaife, S. C. Hardiman, D. M. Mitchell, N. Butchart, M. P. Baldwin, and L. J. Gray, 2015: Stratospheric influence on tropospheric jet streams, storm tracks and surface weather. *Nat. Geosci.*, **8**, 433–440, doi:10.1038/ngeo2424.

Kirtman, B. P., and Coauthors, 2014: The North American Multimodel Ensemble: Phase-1 seasonal-to-interannual prediction; Phase-2 toward developing intraseasonal prediction. *Bull. Amer. Meteor. Soc.*, **95**, 585–601, doi:10.1175/BAMS-D-12-00050.1.

Kryjov, V. N., 2012: Seasonal climate prediction for North Eurasia. *Environ. Res. Lett.*, **7**, 015203, doi:10.1088/1748–9326/7/1/015203.

Lau, N.-C., 1985: Modeling the seasonal dependence of the atmospheric response to observed El Niños in 1962–76. *Mon. Wea. Rev.*, **113**, 1970–1996, doi:10.1175/1520-0493(1985)113<1970:MTSDOT>2.0.CO;2.

Meinshausen, M., and Coauthors, 2011: The RCP greenhouse gas concentrations and their extensions from 1765 to 2300. *Climatic Change*, **109**, 213–241, doi:10.1007/s10584-011-0156-z.

Palin, E. J., A. A. Scaife, E. Wallace, E. C. D. Pope, A. Arribas, and A. Brookshaw, 2016: Skillful seasonal forecasts of winter disruption to the U.K. transport system. *J. Appl. Meteor. Climatol.*, **55**, 325–344, doi:10.1175/JAMC-D-15-0102.1.

Rayner, N. A., D. E. Parker, E. B. Horton, C. K. Folland, L. V. Alexander, D. P. Rowell, E. C. Kent, and A. Kaplan, 2003: Global analyses of sea surface temperature, sea ice, and night marine air temperature since the late nineteenth century. *J. Geophys. Res.*, **108**, 4407, doi:10.1029/2002JD002670.

Riddle, E. E., A. H. Butler, J. C. Furtado, J. L. Cohen, and A. Kumar, 2013: CFSv2 ensemble prediction of the wintertime Arctic Oscillation. *Climate Dyn.*, **41**, 1099–1116, doi:10.1007/s00382-013-1850-5.

Rienecker, M. M., and Coauthors, 2011: MERRA: NASA's Modern-Era Retrospective Analysis for Research and Applications. *J. Climate*, **24**, 3624–3648, doi:10.1175/JCLI-D-11-00015.1.

Ropelewski, C. F., and M. S. Halpert, 1986: North American precipitation and temperature patterns associated with the El Niño/Southern Oscillation (ENSO). *Mon. Wea. Rev.*, **114**, 2352–2362, doi:10.1175/1520-0493(1986)114<2352:NAPATP>2.0.CO;2.

Scaife, A. A., and J. R. Knight, 2008: Ensemble simulations of the cold European winter of 2005–2006. *Quart. J. Roy. Meteor. Soc.*, **134**, 1647–1659, doi:10.1002/qj.312.

——, ——, G. K. Vallis, and C. K. Folland, 2005: A stratospheric influence on the winter NAO and North Atlantic surface climate. *Geophys. Res. Lett.*, **32**, L18715, doi:10.1029/2005GL023226.

——, and Coauthors, 2014: Skillful long-range prediction of European and North American winters. *Geophys. Res. Lett.*, **41**, 2514–2519, doi:10.1002/2014GL059637.

——, and Coauthors, 2016: Seasonal winter forecasts and the stratosphere. *Atmos. Sci. Lett.*, **17**, 51–56, doi:10.1002/asl.598.

Shukla, J., 1998: Predictability in the midst of chaos: A scientific basis for climate forecasting. *Science*, **282**, 728–731, doi:10.1126/science.282.5389.728.

Sigmond, M., J. F. Scinocca, V. V. Kharin, and T. G. Shepherd, 2013: Enhanced seasonal forecast skill following stratospheric sudden warmings. *Nat. Geosci.*, **6**, 98–102, doi:10.1038/ngeo1698.

Stockdale, T. N., D. L. T. Anderson, J. O. S. Alves, and M. A. Balmaseda, 1998: Global seasonal rainfall forecasts using a coupled ocean–atmosphere model. *Nature*, **392**, 370–373, doi:10.1038/32861.

——, F. Molteni, and L. Ferranti, 2015: Atmospheric initial conditions and the predictability of the Arctic Oscillation. *Geophys. Res. Lett.*, **42**, 1173–1179, doi:10.1002/2014GL062681.

Thompson, D. W. J., M. P. Baldwin, and J. M. Wallace, 2002: Stratospheric connection to Northern Hemisphere wintertime weather: Implications for prediction. *J. Climate*, **15**, 1421–1428, doi:10.1175/1520-0442(2002)015<1421:SCTNHW>2.0.CO;2.

Ting, M., Y. Kushnir, R. Seager, and C. Li, 2009: Forced and internal twentieth-century SST trends in the North Atlantic. *J. Climate*, **22**, 1469–1481, doi:10.1175/2008JCLI2561.1.

Tripathi, O. P., and Coauthors, 2015: The predictability of the extratropical stratosphere on monthly time-scales and its impact on the skill of tropospheric forecasts. *Quart. J. Roy. Meteor. Soc.*, **141**, 987–1003, doi:10.1002/qj.2432.

Vecchi, G., and Coauthors, 2014: On the seasonal forecasting of regional tropical cyclone activity. *J. Climate*, **27**, 7994–8016, doi:10.1175/JCLI-D-14-00158.1.

Venzke, S., M. R. Allen, R. T. Sutton, and D. P. Rowell, 1999: The atmospheric response over the North Atlantic to decadal changes in sea surface temperature. *J. Climate*, **12**, 2562–2584, doi:10.1175/1520-0442(1999)012<2562:TAROTN>2.0.CO;2.

Wang, B., R. Wu, and X. Fu, 2000: Pacific–East Asian teleconnection: How does ENSO affect East Asian climate? *J. Climate*, **13**, 1517–1536, doi:10.1175/1520-0442(2000)013<1517:PEATHD>2.0.CO;2.

Yang, X., G. A. Vecchi, R. G. Gudgel, T. Delworth, and S. Zhang, 2015: Seasonal predictability of extratropical storm tracks in GFDL's high-resolution climate prediction model. *J. Climate*, **28**, 3592–3611, doi:10.1175/JCLI-D-14-00517.1.

Zhang, S., M. J. Harrison, A. Rosati, and A. T. Wittenberg, 2007: System design and evaluation of coupled ensemble data assimilation for global oceanic climate studies. *Mon. Wea. Rev.*, **135**, 3541–3564, doi:10.1175/MWR3466.1.